

STATUS OF STRANGENESS-FLAVOR SIGNATURE OF QGP*

JAN RAFELSKI

Department of Physics, University of Arizona, Tucson, AZ85721, USA

JEAN LETESSIER

Laboratoire de Physique Théorique et Hautes Energies
Université Paris 7, 2 place Jussieu, 75251 Cedex 05, France

(Received October 13, 2006)

Is the new state of matter formed in relativistic heavy ion collisions the deconfined quark–gluon plasma? We survey the status of several strange hadron observables and discuss how these measurements help understand the dense hadronic matter.

PACS numbers: 12.38.Mh, 24.10.Pa, 25.75.-q

1. Introduction

Matter made of free quarks has been discussed in literature for more than 30 years. For further theoretical details and historical developments we refer to the “Theoretical Foundations” collection of QGP articles [1]. Today, many believe that a new state of matter made of free quarks has been formed in relativistic nuclear collisions. Is this “really” the interacting plasma of QCD quanta, quarks and gluons (QGP), formed and present in a limited domain of space and time, where quarks and gluons are propagating constrained by external “frozen vacuum”, which abhors color? Before proceeding to more specific matters, we will make a few general remarks.

We shall discuss in these notes the yields of a diversity of strange hadronic particles produced in relativistic heavy ion collisions, and consider also theoretical models of strangeness production in QGP. In the analysis of (strange) hadron yields we use the statistical hadronization model (SHM) to connect properties of matter with yields of particles (or *vice versa*). We note that

* Presented at the XLVI Cracow School of Theoretical Physics, Zakopane, Poland May 27–June 5, 2006.

experiments detect reliably just a small fraction of all hadrons of interest. In order to have global and detailed information about the properties of the dense matter source of these hadrons, an extrapolation must be made to cover production yields of all particles.

The yield of measured particles are obtained from their spectra, which are extrapolated to allow the integration over the full phase space. This introduces considerable systematic uncertainty, but reduces greatly the dependence on the dynamics of fireball evolution at time of hadronization. In this work, we address quantitatively either the m_{\perp} -integrated rapidity density dN/dy , or the total particle yields, referring sometimes the spectral m_{\perp} shape. Even in this reduced case, considering the complexity of hadronization, and the very rich experimental data set, considerable effort is required to complete the data analysis. For this reason, we helped develop a hadronization tool SHARE (Statistical HAdronization with REsonances), a suite of numeric analysis programs which is available in the public domain [2]. SHARE is used in all analysis presented here. SHARE encompasses many other statistical hadronization models (SHM), which arise as special cases in SHARE set of parameters.

As the above implies, there are several different approaches one can take in the study of particle yields using SHM. In our opinion, SHM is a physics-motivated model extrapolating from a subset to all particle yields. Therefore, we take the most elaborate version of the SHM model to compare with experiment: the results we present are obtained allowing for the full chemical non-equilibrium in the analysis of hadron yield data.

We present here the key strangeness QGP observables and look at the results with two questions in mind: has the experimental result been predicted to be a QGP consequence? Is an alternative explanation of the data available today, which does not contradict the behavior of the data being explained? We will also discuss how understanding of strangeness production at SPS and RHIC helps to prepare for the LHC energy range, and the low energy RHIC run.

We address in turn the $\bar{\Lambda}/\bar{p}$ (next section), strange (anti)baryon enhancement at SPS and RHIC (Section 3), The K^+/π^+ -horn (Section 4). In this context, we expand on the observation of a change in the reaction mechanism, favoring baryons at energies at or above the K^+/π^+ -peak. We then introduce the bulk observable, strangeness per entropy s/S in Section 5, and show how it helps evaluate the ratio of degrees of freedom present. We show how s/S can be computed at RHIC and LHC and present results showing independence of the result from initial conditions other than entropy content dS/dy . In Section 7, we discuss strange hadron resonances and their importance to the diagnosis of QGP. We close the discussion, in Section 8, with a short outlook at future developments.

2. Ratio of $\bar{\Lambda}$ with \bar{p} at SPS

The first proposed strangeness and hadron yield ratio signature of QGP has been the relative yield of $\bar{\Lambda}$ and \bar{p} [3, 4]. After cancellation of combinatorial and phase space factors, this ratio is determined by relative quark yields available at hadronization. If no QGP were formed, one could at best hope for chemical equilibrium yields in the hadron gas matter, but especially at relatively low reaction energies this requires a magic touch, the chemical equilibration of strangeness in hadron born reactions.

For both particles considered we include, aside of directly produced $\bar{\Lambda}$, \bar{p} , the yields of more massive resonances which decay into these particles. SHARE accounts for this important effect. However, we present first the more intuitive historical line of thought: we assume that the resonance contributions multiply both $\bar{\Lambda}$ and \bar{p} by similar enhancement factors. This being the case, resonance effect can be ignored at first when considering the $\bar{\Lambda}/\bar{p}$ ratio.

In a baryon-rich QGP environment, the light antiquark \bar{u} , \bar{d} abundances are suppressed. This is easily understood as result of \bar{u} , \bar{d} annihilation on u , d excess present where baryons are present. In the statistical hadronization model, this effect is described by the baryochemical potential $\mu_b = 3(\mu_u + \mu_d)/2 = 3\mu_q$. However, the strange antiquark yield \bar{s} is also suppressed by the strange quark mass. Integrating the particle phase space characterized by a production temperature T_h (hadronization temperature) we find:

$$\begin{aligned} \left. \frac{\bar{\Lambda}}{\bar{p}} \right|_{\text{QGP}} &= \frac{N_{\bar{s}} N_{\bar{u}} N_{\bar{d}}}{N_{\bar{u}} N_{\bar{u}} N_{\bar{d}}} \simeq \frac{\gamma_s^{\text{QGP}}}{\gamma_q^{\text{QGP}}} \frac{1}{2} \frac{m_s^2}{T_h^2} K_2 \left(\frac{m_s}{T_h} \right) e^{(\mu_u^{\text{QGP}} - \mu_s^{\text{QGP}})/T_h} \\ &= \frac{\gamma_s^{\text{QGP}}}{\gamma_q^{\text{QGP}}} 0.9 e^{(\mu_u^{\text{QGP}} - \mu_s^{\text{QGP}})/T_h}. \end{aligned} \quad (1)$$

The last equality follows for the currently accepted value $m_s/T_h \simeq 0.7$.

The relative yield originating in the hadron phase comprises, in place of strange quark mass suppression, the hadron phase space suppression factor:

$$\begin{aligned} \left. \frac{\bar{\Lambda}}{\bar{p}} \right|_{\text{HG}} &= \frac{\gamma_s^{\text{HG}}}{\gamma_q^{\text{HG}}} \left(\frac{m_{\bar{\Lambda}}}{m_{\bar{p}}} \right)^{3/2} e^{-(m_{\bar{\Lambda}} - m_{\bar{p}})/T_f} e^{(\mu_u^{\text{HG}} - \mu_s^{\text{HG}})/T_f} \\ &= \frac{\gamma_s^{\text{HG}}}{\gamma_q^{\text{HG}}} 1.3 e^{-180 \text{ MeV}/T_f} e^{(\mu_u^{\text{HG}} - \mu_s^{\text{HG}})/T_f}. \end{aligned} \quad (2)$$

In the range $T_f \simeq 160 \pm 20$ MeV, the HG yield is significantly smaller compared to the relative yield from QGP. Moreover, in HG the multiplicative factor γ_s/γ_q , will be well below unity at low collision energy. As a side

remark, note that the analysis of the experimental data suggests that this chemical equilibration factor reaches unity for most central and most energetic SPS reactions which is evidence for a new production mechanism of all particles.

An important and self-evident result is that, using hadron phase space, it is indeed impossible to ever obtain for $\bar{\Lambda}/\bar{p}$ a value that exceeds unity. However, the situation is different when QGP hadronizes. Let us recall the equilibrium hadronization conditions:

$$T_h \simeq T_f, \quad \langle s + \bar{s} \rangle^Q \simeq \langle s + \bar{s} \rangle^H, \quad S^Q \simeq S^H, \quad \mu_u^Q - \mu_s^Q = \mu_u^H - \mu_s^H, \quad (3)$$

here S is the entropy and both s and S can be understood to be rapidity density. We abbreviate above Q for QGP and H for HG. Moreover, irrespective of question of phase transition, for the purpose of comparison of production yields one normally assumes that chemical potentials are measured and thus yields are compared at a given value obtained from experimental data:

$$\mu_u - \mu_s = \text{const.} \quad (4)$$

In either case much of enhancement of $\bar{\Lambda}/\bar{p}$ (and other strange antibaryon relative yield in QGP compared to HG) is due to the reduced threshold of strangeness in QGP compared to HG.

This argument correctly describes the yields of dominant fractions of (strange) particles which carry most of strangeness. For the rarely produced particles, *e.g.* antibaryons produced are at low reaction energy, the situation is more involved. At the onset of global hadronization, $\mu_s^{\text{QGP}} \simeq 0$. This is so since in QGP at first $s - \bar{s} = 0$, and strangeness is not clustered in baryon like objects in plasma. Considering that the HG phase is asymmetric at a given baryon number, there is a buildup of μ_s^{QGP} with time, reversing with time the asymmetric strangeness emission in hadrons.

For conditions we consider, the initially preferentially emitted particles are carriers of \bar{s} -quarks. $\bar{\Lambda}$ (and $(q\bar{s})$ kaons) is emitted at first with preference. As time progresses this leads to an increase in μ_s^{QGP} in plasma phase such that symmetric emission and later s -quark emission dominance ensues, assuring that strangeness conservation $s - \bar{s} = 0$ is achieved among all produced particles by the end of hadronization. However, it has also been speculated that the early asymmetric emission of particles with $\bar{s} > s$ could lead to the formation of a strangeness enriched residual matter [6]. Extensive searches for this effect failed to confirm this reaction model. What is perhaps instead happening is that at some point μ_s^{QGP} is large enough such that emission of particles with $s > \bar{s}$ dominates.

At the beginning of the process of hadronization, the production of $\bar{\Lambda}$ (and $\bar{\Xi}, \bar{\Omega}$) is enhanced by $\mu_s^{\text{QGP}} = 0$. Once produced, particles do not disappear, and thus QGP property $\mu_s^{\text{QGP}} = 0$ is imprinted on the enhanced yield

of rarely produced strange antibaryons, which are predominantly produced in the early time stage of QGP hadronization. Thus,

$$\left. \frac{\bar{\Lambda}}{\bar{p}} \right|_{\text{QGP}} \simeq 0.9 \lambda_u^{\text{QGP}}, \quad \lambda_u^{\text{QGP}} = e^{(\mu_u^{\text{QGP}}/T_h)}. \quad (5)$$

It is well understood that the value of quark fugacity λ_u^{QGP} at hadronization increases with decreasing reaction energy. This implies that with decreasing reaction energy the relative yield $\bar{\Lambda}/\bar{p}$ increases, which at first sight is an unexpected result.

Beyond this qualitative discussion, originally presented more than 25 years ago, a quantitative prediction which includes all resonance decays is shown in Fig. 47 of our *Acta Physica Polonica B* review article from 1996 [5], which is reproduced with figure caption, see Fig. 1. The energy scale E/B (fireball energy content per baryon) is somewhat unusual, yet it corresponds almost exactly to $\sqrt{s_{NN}}$, the center of momentum frame nucleon pair reaction energy. Namely, for stopping of energy being 50% of participant stopping, the fireball energy content per baryon E/B , seen in Fig. 1, would be just the CM energy per colliding nucleon pair. Study of energy and participant number content in the fireball matter formed at low energy SPS reactions suggest that 50% relative stopping is the right order of magnitude.

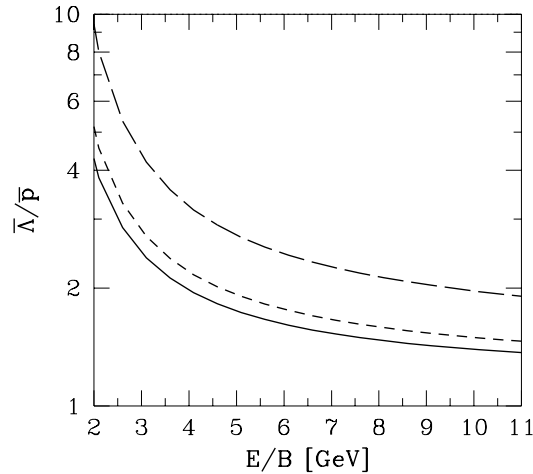


Fig. 1. Strange antibaryon ratio $\bar{\Lambda}/\bar{p}$, as function of E/B in a QGP-fireball for $\gamma_s = 1$; solid lines are for full phase space coverage, short dashed line for particles with $p_{\perp} \geq 1$ GeV and long dashed line for particles with $m_{\perp} \geq 1.7$ GeV (reproduced from *Acta Physica Polonica B* [5]).

The result seen in Fig. 1 is not surprising, following on our qualitative discussion, we see how the ratio $\bar{\Lambda}/\bar{p}$ is increasing with decreasing reaction energy. It is of some interest to compare this result with the AGS and the SPS experimental results. The data analysis has been evolving. The results are shown in Fig. 2, based on compilation of data and theoretical results by the NA49 collaboration [7]. We see that the central rapidity ratio $\bar{\Lambda}/\bar{p}$ is well above unity at all available reaction energies. With decreasing reaction energy, this ratio increases, just as it is expected in our above discussion. The fact that to lowest considered collision energies and smallest reaction systems at AGS this trend persists (within the quite large error bars) could suggest that QGP formation followed by slow and continuous hadronization is the reaction mechanism governing the production of strange antibaryons at relatively low AGS energies.

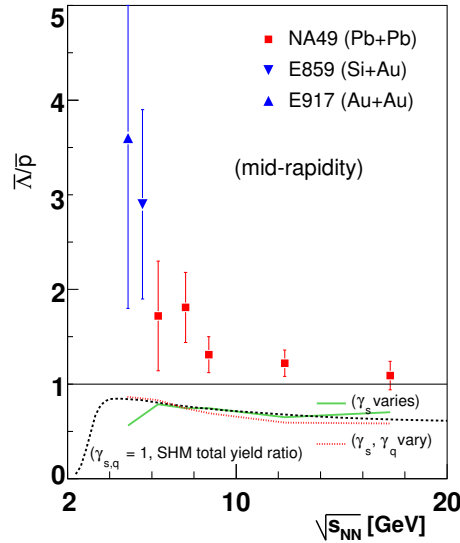


Fig. 2. Top: observed mid-rapidity particle yield ratio $\bar{\Lambda}/\bar{p}$ as function of nucleon-nucleon reaction energy $\sqrt{s_{NN}}$. Bottom: statistical QGP hadronization total yield ratios in different QGP breakup scenarios. NA49 compilation of own, AGS data and theoretical results.

In the bottom of Fig. 2, the bulk matter predictions are shown, based on global SHM fits to the experimental data carried out by different groups (including our own results), under differing scenarios, all theoretical results have been assembled by the NA49 group and we refer to this work for further discussion and references. Comparing data with bulk yields we see that the additional enhancement of $\bar{\Lambda}/\bar{p}$ we attribute to dynamically evolving μ_s is

most pronounced at lowest reaction energies. In fact, for the highest reaction energies, where sudden breakup of the QGP fireball is assured, the discrepancy between bulk hadronization and experimental data could perhaps be accounted for by conventional means. Specifically, the experimental $\bar{\Lambda}/\bar{p}$ ratio needs to be reduced to correct for the included weak decays $\bar{\Xi} \rightarrow \bar{\Lambda}$ which are not included in the SHM models. Moreover, the thermal rapidity distribution of $\bar{\Lambda}$ is narrower than that of \bar{p} , which enhances the central rapidity ratio compared to the 4π -yields shown in the theoretical part of the figure. On the other hand, the trend of the data at low energies is quite clear, despite the large error bars.

We conclude: $\bar{\Lambda}/\bar{p} > 1$ ratio, rising with decreasing reaction energy, has been predicted to arise in hadronization of QGP. No other explanation of this behavior is known to us. An alternate explanation would have to address both the magnitude of the effect and its energy dependence. The available data is consistent with QGP; however, good experimental results are needed to confirm this intriguing trend.

On the other hand, we note that the absolute yields $\bar{\Lambda}$, and \bar{p} are not large. At the top AGS energy (11.6 A GeV for central Au–Au collisions), in the most central reactions, one $\bar{\Lambda}$ or \bar{p} will be produced in one out of 100 Au–Au collisions. There are important kinetic rescattering processes which can generate a shift $\bar{\Lambda} \leftrightarrow \bar{p}$ inducing suppression, or enhancement of $\bar{\Lambda}$ or \bar{p} . Qualitative kinetic model rescattering arguments favor $\bar{\Lambda}$ over \bar{p} yield: the annihilation cross section on baryon matter is smaller for $\bar{\Lambda}$. The strangeness exchange cross reaction is exothermic for $\bar{p} + (q\bar{s}) \rightarrow \bar{\Lambda} + (q\bar{q})$. Thus, kinetic rescattering in HG could increase the ratio $\bar{\Lambda}/\bar{p}$ beyond relative chemical equilibrium yield.

Such dynamical effects are not common but must be investigated before we conclude that QGP is formed at top AGS energies. When good data at AGS reaction energy becomes available, $\bar{\Lambda}/\bar{p}$ is one of the observables meriting very careful experimental and theoretical study. This is the low reaction energy probe of QGP most resembling J/Ψ suppression: the signal is very clean, but must be carefully considered for competing effects.

3. Strange (anti)baryon enhancement at SPS and RHIC

CERN experiments WA97 and NA57 have focused on the study of the systematics of the strange (anti)baryon enhancement with reaction energy, and centrality in Pb–Pb collisions. Λ , Ξ and Ω and antiparticle yields have been measured at central rapidity y and medium transverse momentum p_{\perp} as functions of the centrality of the collision. Comparing the yields in Pb–Pb to those in p Be interactions, considerable enhancement of yield per participant is observed. This enhancement increases linearly with the centrality, and

geometrically with the strangeness content in hyperons, reaching a factor of about 20 for the $\Omega + \bar{\Omega}$ in the central Pb–Pb collisions. Recently, the final results for the centrality dependence of (anti)hyperon production in Pb–Pb, p Pb and p Be collisions at A GeV/ c have been reported [8]. The open symbols, in Fig. 3, show these results, which follow the pattern predicted in the recombination-hadronization model [9]. The enhancement rises, both with the strangeness content in the hadron, and with the participant number A (centrality), that is the size of the reaction region. The magnitude of the enhancement is nearly the same as seen at much lower SPS energy range.

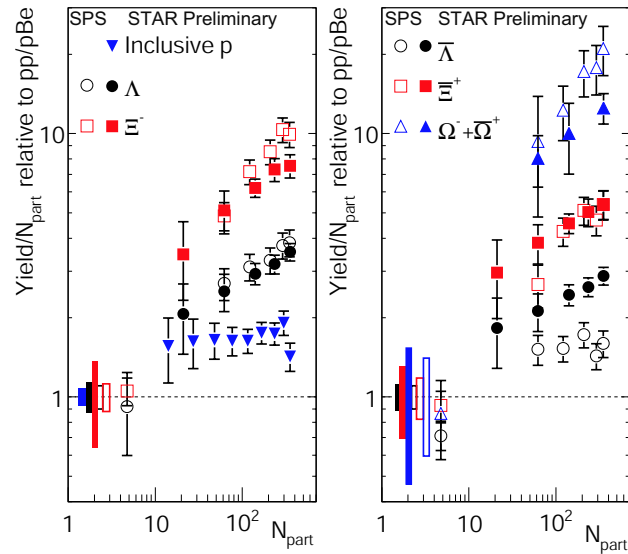


Fig. 3. Yields per participant N_{part} , for NA57-SPS Pb–Pb $\sqrt{s_{NN}} = 17.3$ GeV (open symbols) relative to pBe and for STAR-RHIC Au–Au $\sqrt{s_{NN}} = 200$ GeV (filled symbols) relative to pp . On left baryons, on right antibaryons and $\Omega + \bar{\Omega}$ (triangles), circles are Λ and $\bar{\Lambda}$, squares are Σ^- and $\bar{\Sigma}^+$. Error bars represent those from the heavy-ion measurement. Ranges for pp and pBe reference data indicate the statistical and systematic uncertainty. After [14].

There are further features of the WA97 and NA57 experimental results which are particularly important: the enhancement seen at 40 A GeV/ c is very similar, nearly identical, particle by particle, as seen at 158 A GeV/ c [10,11] except for the most peripheral class of events. We read this result to mean that the peripheral 40 A GeV/ c reactions do not always reach deconfinement. The final experimental results differ little from the preliminary conference reports which we discussed at this school in 2003 [12] and in 1999 [13]. For this reason, we focus discussion of this enhancement pattern at RHIC, and the comparison of RHIC with SPS.

The solid symbols, in Fig. 3, correspond to the most recent STAR results obtained at $\sqrt{s_{NN}} = 200$ GeV [14]. The yield of (multi)strange baryons $\Lambda(uds)$, $\Xi^-(dss)$ and antibaryons per participant N_{part} in the reaction, divided by a reference yield obtained in pp reactions is shown. Within error, considering also the base yield, the enhancement at RHIC and SPS appears the same. However, there are two issues to consider:

- (a) The enhancement computed by NA57 is based on $p\text{Be}$, where some enhancement of Λ is expected to be present, as compared to pp results. The NA49 SPS experiment has just reported Λ enhancement evaluated with reference to pp [15]. In this more directly comparable case, the SPS Λ -enhancement comes to be factor 5–6 (rather than 4–5) in most central Pb–Pb reactions.
- (b) The behavior of $\bar{\Lambda}$ enhancement at SPS breaks the ranks in that it is seen to be nearly flat as function of centrality, and it is smaller at SPS than at RHIC.

We conclude that the enhancement pattern of Λ and $\bar{\Lambda}$ is influenced by the prevailing baryon density, for $\bar{\Lambda}$ the enhancement is greater at RHIC where the baryon density is smaller than at SPS, while the reverse is true for Λ . This baryochemical potential effect is mostly erased considering Ξ^- , $\bar{\Xi}^+$, but is visible within the error bar. The enhancement of $\Omega + \bar{\Omega}$ is largest, since production of these particles is very difficult in the elementary reactions, especially so at the lower SPS energy.

The interpretation we pursue is that the strange antibaryon enhancement is due to an increased yield density of strange quarks at hadronization, growing within the geometric source size, the increase driven by the longer lifespan. The gradual increase of the enhancement over the range of N_{part} is an important indicator of the kinetic strangeness production mechanism. We return to this in Section 6, in the strangeness yield analysis as function of centrality [16]. This enhancement at RHIC is in fact fully understood. We compare the theoretical predictions with the experimental results for Λ and Ξ^- on left and $\bar{\Lambda}$ and $\bar{\Xi}^+$ at RHIC in Fig. 4. Note that the normalization of the enhancement is different [17], as compared to Fig. 3. This has occurred since the interpretation of the reference pp data changed. However, this vertical shift (in a log-figure) does not affect the comparison of theory and experiment since both use the same experimental pp yield normalizer to define the enhancement. We note that data in Fig. 3 is “newer”.

The theoretical lines, in Fig. 4, follow from study of strangeness yield in these reactions based mainly on PHENIX single strange hadron results [18], and application of statistical hadronization model using these results [19], to predict the yields shown [16]. For most peripheral collisions, this study is not

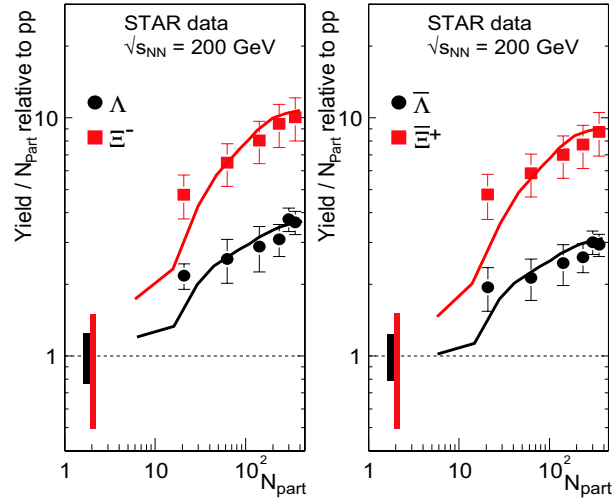


Fig. 4. Yields per participant N_{part} relative to pp of Λ and Ξ^- on left and $\bar{\Lambda}$ and $\bar{\Xi}^+$ on right in Au+Au collisions at $\sqrt{s_{NN}} = 200$ GeV [17] (compare Fig. 3). Our theoretical results [16] are for chemical non-equilibrium and are normalized to the same pp experimental results.

entirely applicable, since the SHM fit to the data is not fully reliable. This is the “kink” in the theoretical curves seen in Fig. 4. An important help in understanding these results is the gradual growth of the enhancement with centrality. As we see, the trend is quantitatively consistent with strangeness yield growth (see Section 6). Both the energy and centrality dependence of the enhancement contradicts the canonical suppression model, which reinterprets this enhancement as being due to reference data suppression [20].

4. From baryons to mesons

The enhancement of (strange) (anti)baryons we just presented is also due to enhanced production of baryons as compared to mesons when AA reactions are compared to pp reactions. Fig. 5 shows the ratios of \bar{p}/π and $\bar{\Lambda}/K_S$ from central Au–Au collisions at $\sqrt{s_{NN}} = 130$, and 200 GeV measured by PHENIX [18] and STAR [21–23].

We recognize that the formation of mesons and baryons occurs by a different mechanism than in the elementary pp reactions. In particular, the large baryon to meson ratio, seen in Fig. 5, cannot be accommodated by the conventional string fragmentation scheme developed for the elementary e^+e^- and pp reactions. The quark recombination models [24, 25] provided a satisfactory description of the particle yields, in particular, the large production of anti baryons in the intermediate p_{\perp} region.

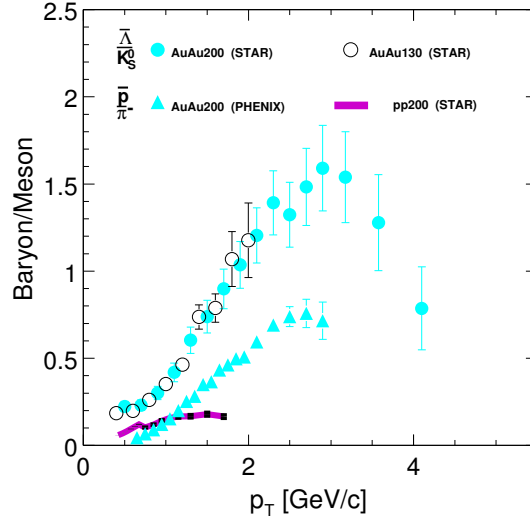


Fig. 5. Ratios of $\bar{\Lambda}$ to K_S^0 from Au–Au and pp collisions (STAR) and \bar{p} to π from Au–Au collisions (PHENIX) as a function of transverse momentum (p_\perp). In addition to resonance contributions in all hadrons, the $\bar{\Lambda}$ includes contributions from Σ^0 decays.

Within the statistical hadronization model, when chemical equilibrium is assumed, the relative ratio of baryons to mesons is fixed, and varies along with hadronization temperature T . When chemical nonequilibrium ideas are introduced, the parameter controlling the relative abundance of baryons with respect to mesons is γ_q ,

$$\frac{\text{Baryons}}{\text{Mesons}} = \gamma_q R_P \left(T, \frac{\gamma_s}{\gamma_q}, \frac{\mu_i}{T} \right), \quad (6)$$

where μ_i are chemical potentials, and γ_s/γ_q is the relative strangeness to light quark phase space occupancy. There is excess baryon-antibaryon pair yield over chemical equilibrium for $\gamma_q > 1$, expected when the source of particles is a very dense deconfined quark state. Conversely, for low energies or small systems, we expect $\gamma_q < 1$. The value $\gamma_q = 1$ can be established when there is time to scatter and equilibrate the yields of mesons and baryons, which in general is not the case in all reactions described here.

Consideration of chemical nonequilibrium and the possibility that in some reactions $\gamma_q > 1$, and in others $\gamma_q < 1$, provides an opportunity to describe the energy dependence of particle production, studied by the experiment NA49 [26]. This has as special objective the interpretation of the K^+/π^+ ratio [27,28], which shows a pronounced energy dependent structure, see Fig. 6.

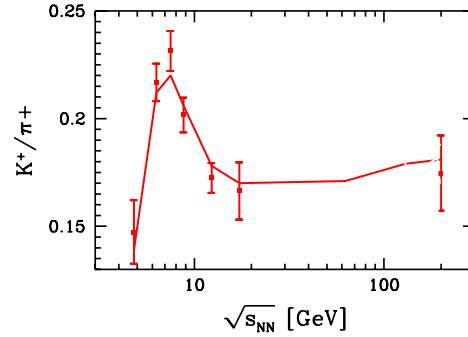


Fig. 6. K^+/π^+ ratio of NA49 experiment [27, 28]. Solid line: Result of chemical nonequilibrium hadron production analysis [26].

The rapid rise in the $K^+/\pi^+ \propto \bar{s}u/\bar{d}u$ ratio is due to the more rapid increase in \bar{s} than \bar{d} when the baryon density is very high. The decrease beyond the peak is driven by a reduction of baryon stopping with increasing reaction energy, at which time there is a faster increase in the \bar{d} yield. In the SHM description the key ingredient needed to obtain this behavior, in consistency with all particle yields, is the switch-over at the peak of the ratio, from $\gamma_q < 1$ to $\gamma_q > 1$. The gradual rise of K^+/π^+ at high energy is associated with an increase of γ_s/γ_q .

The observable K^+/π^+ has been long considered as a signature of strangeness enhancement [29]. It turned out to also be a signature of anti-quark suppression in high baryon density fireballs created at low reaction energy. Moreover, there appears to be a change in hadronization mechanism associated with the intermediate peak in K^+/π^+ . The advancement of this most interesting physics result is mainly due to the diligent work of Gaździcki [27].

5. Strangeness per entropy

Individual particle yields are in general probing conditions prevailing at the time of QGP hadronization. However, bulk fireball properties reach more deeply into the history of QGP evolution. Of particular interest is the ratio strangeness per entropy s/S . Studies of QGP suggest that entropy and to a lesser extent strangeness yields are produced in the earliest stages of the heavy ion reaction. In the next Section 6, we will show how “deep” strangeness probes. In this section, we look at the qualitative features of this observable.

The deconfined state is rich in both in entropy and strangeness. The enhancement of entropy S arises because the color bonds are broken and gluons can be created. Enhancement of strangeness s arises because the mass

threshold for strangeness excitation is considerably lower in QGP than in hadron matter. While entropy S determines the hadron multiplicity content, strangeness s determines strange hadron content. Thus, to measure s/S , we need to have measured particle yields which comprise much of the total strange and non-strange hadron multiplicity.

In QGP, strangeness s originates primarily in gluon based reactions, *e.g.*, $GG \rightarrow s\bar{s}$, and higher order gluon related processes. Gluons are the source of strangeness; their presence requires deconfinement, and is a result of entropy production, *i.e.*, excess entropy S content. It is generally believed that the entropy production is completed after first 0.5–1 fm/ c reaction time, at which time the parton matter has turned into the thermalized QGP phase. Strangeness is produced shortly after. We have been able to unravel much of mystery behind strangeness production (see Section 6). However, mechanisms of entropy formation are not understood.

We estimate the expected magnitude of s/S . For thermally equilibrated non-interacting QGP phase at a temperature T_s at which formation of strangeness essentially has ended:

$$\frac{s}{S} \equiv \frac{\rho_s}{\sigma} = \frac{(3/\pi^2)T_s^3(m_s/T_s)^2 K_2(m_s/T_s)}{(32\pi^2/45)T_s^3 + n_f[(7\pi^2/15)T_s^3 + \mu_q^2 T_s]} = \frac{0.03}{1 + 0.054(\ln \lambda_q)^2}. \quad (7)$$

Here, we used for the number of flavors $n_f = 2.5$ and $2m_s/T_s = 1$. We see that the result is a slowly changing function of λ_q ; for large $\lambda_q \simeq 4$, present at modest SPS energies, the value of s/S is reduced by 10% as compared to $\lambda_q \simeq 1$ applicable to LHC and RHIC. Considering the slow dependence on $x = m_s/T \simeq 1$ of $W(x) = x^2 K_2(x)$ there is a minor residual dependence on the value of T_s .

The dependence on the degree of chemical equilibration which dominates is easily obtained by separating the different degrees of freedom:

$$\frac{s}{S} = 0.03 \frac{\gamma_s^{\text{QGP}}}{0.38\gamma_G^{\text{QGP}} + 0.12\gamma_s^{\text{QGP}} + 0.5\gamma_q^{\text{QGP}} + 0.054\gamma_q^{\text{QGP}}(\ln \lambda_q)^2}. \quad (8)$$

Given Eq. (8), we expect to see a gradual increase in s/S as the QGP source of particles approaches chemical equilibrium with increasing collision energy and/or increasing volume.

How does this simple prediction compare to experiment? A precise measurement of s/S is not easy, since it requires measurement of several particles species to considerable precision. Analysis of existent data was done as a function of centrality [19], and as a function of reaction energy [26]. The centrality study included 11 centrality bins of Au–Au at $\sqrt{s_{NN}} = 200$ GeV for which dN/dy for π^\pm , K^\pm , p and \bar{p} at $y_{\text{CM}} = 0$ have been presented in Table VIII, in Ref. [18] (PHENIX). These 6 particle yields and their ratios

change rapidly as function of centrality. In addition results from STAR for $K^*(892)/K^-$ [30], and ϕ/K^- [31] which show minor centrality dependence were used.

Supplemental constraints (ratio $\pi^+/\pi^- = 1. \pm 0.02$, strangeness conservation, electrical charge to net baryon ratio) help to determine the best fit. The 7 SHM parameters (volume per unit of rapidity dV/dy , temperature T , four chemical parameters $\lambda_q, \lambda_s, \gamma_q, \gamma_s$ and the isospin factor λ_{I3} are in this case studied in a systematic fashion as function of impact parameter using 11 yields and/or ratios and/or constraints, containing one (pion ratio) redundancy [19].

χ^2 minimization yielding good significance is easily accomplished, showing good consistency of the data sample. The resulting statistical parameters are seen in Fig. 7, on left, as function of participant number. The full non-equilibrium model $\gamma_q \neq 1, \gamma_s \neq 1$ (full circles, blue) and semi-equilibrium $\gamma_q = 1$ (open circles, green) are shown. From top to bottom the (chemical) freeze-out temperature T , the occupancy factors $\gamma_q, \gamma_s/\gamma_q$ and together in the bottom panel the baryon μ_B and hyperon μ_S chemical potentials.

Each of the panels shows very interesting behavior indicating some particular physics feature at chemical freeze-out. Perhaps the overall most striking result is that, for $A > 20$ only, γ_s/γ_q varies significantly, as does (not shown here) the volume of the reaction domain dN/dV . The scaling of dN/dV with $A^{2/3}$ [16] is expected in a geometric reaction picture. The growth of γ_s/γ_q indicates that with size of the system there is more effective cooking of strangeness. There is no saturation of γ_s as we approach the most central reactions. This is inherent in the data we consider which includes the yields of ϕ , and K^* . This result is consistent with the implication that strangeness is not fully saturated in the QGP source, though it appears over-saturated when measured in the hadron phase space.

The baryo-chemical potential and hyperon potential (bottom panel) is model independent and its nearly constant value indicates that only the reaction energy and not the centrality of the reaction establishes baryon density at hadronization. We find a hadronization temperature which, when we allow for $\gamma_q \neq 1$, is at the level of $T = 140$ MeV, and it rises to $T \simeq 155$ MeV when we force light quark chemical equilibrium on the particle yield fit.

In Fig. 7 (right), we show the same statistical variables as a function of reaction energy. To study the energy dependence, we must assemble several different experimental results from different facilities and experiments [26]. The lowest energy result is from our AGS study [32]; the SPS data we used are from NA49 energy dependence exploration at the CERN-SPS [27]. These results are for the total particle yields. The two highest energy results are based on studies of RHIC data at 130 and 200 GeV at central rapidity and address the dN/dy particle yields, with the highest point corresponding to the results presented at greatest centrality on the left-hand side in Fig. 7.

There are several energy dependent features seen on the right-hand side of Fig. 7. We note the dotted vertical line at energy where some of the SHM parameters undergo a change of behavior. The value of energy corresponds to where NA49 reports a change in the behavior of $K^+/\pi^+ \propto \bar{s}/\bar{d}$.

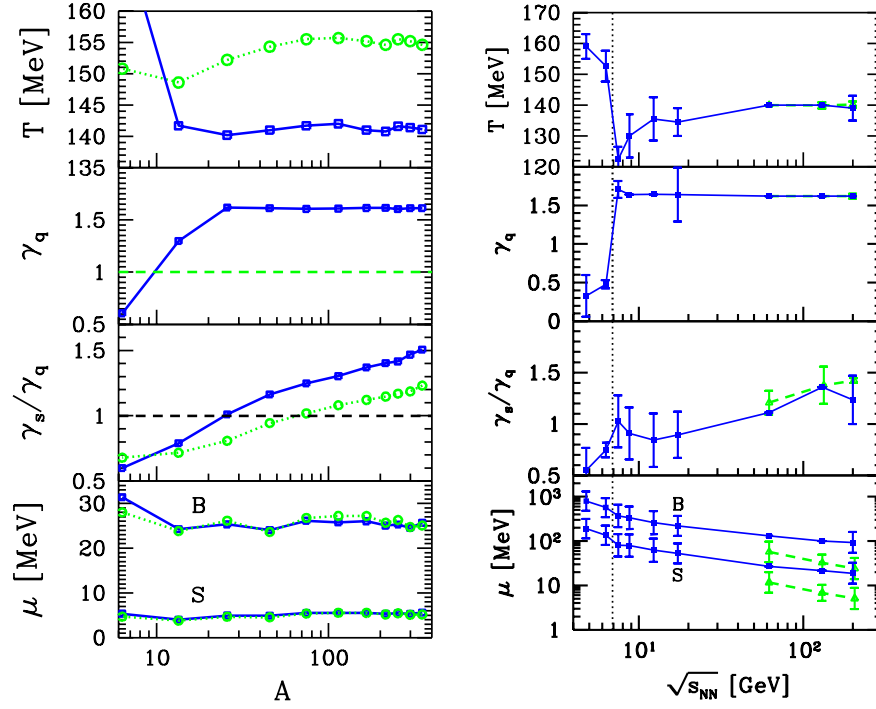


Fig. 7. From top to bottom: temperature T , light quark phase space occupancy γ_q , the ratio of strange to light quark phase space occupancies γ_s/γ_q and the chemical potentials (B for baryochemical μ_B and S for strangeness μ_S). The lines guide the eye. Left: as function of inelastic (wounded) participant number A for top RHIC energy. The full non-equilibrium model $\gamma_q \neq 1, \gamma_s \neq 1$ (filled squares, blue) and semi-equilibrium $\gamma_q = 1$ (open circles, green) are shown. Right: energy $\sqrt{s_{NN}}$ dependence in full chemical nonequilibrium analysis is shown. Note that the additional two highest energy results at RHIC, the on right (filled triangles, green), apply to central rapidity region dN/dy study, while the AGS/SPS and Brahm-RHIC results refer to analysis of the total particle yields (filled squares, blue).

The statistical parameters obtained in the analysis are used to compute s/S as function of centrality [19], and as function of reaction energy [26]. One indeed finds that corresponding to the growth of γ_s/γ_q seen in Fig. 7, the value of s/S grows, reaching nearly the QGP chemical equilibrium value, $s/S \simeq 0.03$ at highest RHIC energy in most central reactions. As a function of centrality at top RHIC energy flat peripheral behavior where $s/S \lesssim 0.02$

at $A < 15$ turns into smoothly increasing s/S reaching $s/S \simeq 0.03$ in most central reactions. As a function of energy near to $\sqrt{s_{NN}} \simeq 6.5$ GeV in most central collisions, there is a change in growth rate of s/S .

The significance of s/S as an observable of QGP is that it is not dependent on the details of the dynamics of hadronization which remain unresolved today. The value is predictable, and helps us understand the degree of chemical equilibration of QGP prior to hadronization. The numeric value for saturated QGP phase is directly proportional to the ratio of the number of strange degrees of freedom to all degrees of freedom in the plasma ($s/S \propto g_s/4g$, see next section). Thus, $s/S \simeq 0.03$ indicates that quark–gluon quanta are active. The smooth rise and the magnitude of s/S are consistent with the QGP reaction picture — a full interpretation of s/S requires better understanding of QGP chemical equilibration, a topic we address next.

6. Strangeness production at RHIC and LHC

The kinetic description of strangeness production can be reorganized to directly evaluate the strangeness yield normalized by entropy yield in plasma, $s(T(\tau))/S(T(\tau))$. In this way, the model dependence on the expansion-dilution phenomenon due to rapid expansion of the QGP phase is considerably reduced. We describe our recent progress in the study of the chemical equilibration at RHIC and LHC [33], and evaluate how this work supports the interpretation of the results of data analysis for s/S presented above.

The temporal evolution of s/S , in an expanding plasma, is governed by:

$$\frac{d}{d\tau} \frac{s}{S} = \frac{A^{gg \rightarrow s\bar{s}}}{(S/V)} [\gamma_g^2(\tau) - \gamma_s^2(\tau)] + \frac{A^{q\bar{q} \rightarrow s\bar{s}}}{(S/V)} [\gamma_q^2(\tau) - \gamma_s^2(\tau)]. \quad (9)$$

When all $\gamma_i \rightarrow 1$, the Boltzmann collision term vanishes, the system has reached chemical equilibrium. The value arrived at for the observable s/S depends on the history of how the system evolves at early stages, and reaches QGP chemical equilibrium for gluons in particular.

In order to be able to solve Eq. (9), a relation between s/S and γ_s is required:

$$\frac{s}{S} = \gamma_s \frac{g_s}{g} \frac{90}{8\pi^4} z^2 K_2(z), \quad z = m_s/T, \quad g_s = 2_s 3_c \left(1 - \frac{k\alpha_s(T)}{\pi} \dots \right). \quad (10)$$

In the initial period, gluons and quarks have not reached chemical equilibrium, thus the actual numerical integrals of Bose and Fermi distributions are dependent on the values $\gamma_{q,g}$. The quark–gluon QCD interactions are introduced to describe the effective degeneracy with precision:

$$g = 2_s 8_c \gamma_g \left(1 - \frac{15\alpha_s(T)}{4\pi} \dots \right) + \frac{7}{4} 2_s 3_c 2_f \gamma_q \left(1 - \frac{50\alpha_s(T)}{21\pi} \dots \right) + \text{strangeness} . \quad (11)$$

The strangeness component is made consistent with g_s in Eq. (10) and the concurrently numerically computed γ_s .

The degeneracies, seen in Eq. (10) for the entropy, include the effect of interactions. Therefore, consistency requires that the interaction effect is also introduced in the strange quark degeneracy g_s , Eq. (10). The value of $k = 2$ applies to massless strange quarks. At $T = 0$ (or said differently, for $m \gg T$) the early study of quark matter self-energy suggests that $k \rightarrow 0$ [34]. The full range $0 < k < 2$ has been explored, the results for $k = 1$ are presented.

We need to model the expansion dynamics of QGP matter. The study of hadronization at RHIC provides a strong constraint on the initial condition and the evolution dynamics of QGP at RHIC. For LHC three modifications are introduced:

1. To account for the greater reaction energy, we increase the initial entropy $dS(\tau_0)/dy$ by factor 4 from 4000 at RHIC to 16000 at LHC. We do not change in the initial value of $s/S|_{\tau_0} = 0.016$; thus, in elementary parton-string interactions, the relative strength of strangeness and non-strange hadron production is left unchanged. This implies an increase in initial strangeness yield by a factor 4 at LHC compared to RHIC.
2. The initial parton thermalization time is reduced from $\tau_0 = 1/4$ fm at RHIC to $\tau_0 = 1/10$ fm at LHC. This does not influence the outcome.
3. In order to accommodate the greater transverse expansion pressure, we increased the maximum transverse flow velocity reached to $v_{\perp} = 0.80 c$. A higher value would increase the over saturation of QGP phase space. Despite a much greater expansion velocity, the evolution time at LHC is significantly longer compared to LHC, with the most central collisions taking up to 30% longer to reach the freeze-out hadronization temperature $T_f = 0.14\text{--}0.17$ GeV. This is due to the greater initial entropy and energy content that takes longer to dilute to the hadronization condition.

Finally, we need to evaluate the invariant strangeness production rate per unit 4-volume, $A^{gg \rightarrow s\bar{s}}$ and $A^{q\bar{q} \rightarrow s\bar{s}}$, see Eq. (9). These are obtained employing the running strength of the QCD coupling, with $\alpha_s(\mu = m_{Z^0}) = 0.118$ evolved to the applicable energy domain μ using the two loops β -function.

Strangeness production, a relatively soft process, can be described perturbatively for two reasons:

- (a) the reaction processes which change the yield of strangeness can compete with the fast $v_{\perp} > 0.5c$ expansion of QGP only for $T > T_s = 220 \text{ MeV} \simeq 2m_s$, for lower temperatures the strange quark yields effectively do not change. T_s is the strange quark chemical freeze-out temperature in QGP. Using the relation $\mu = 2\pi T$, this implies that all strangeness yield evolution occurs for $\mu > 1.4 \text{ GeV}$.
- (b) Because of the magnitude $\alpha_s(\mu = m_{Z^0}) = 0.118$, one can run α_s to the scale of interest, $\mu > 1.2 \text{ GeV}$, and the value $\alpha_s/\pi \lesssim 0.2$ allows perturbative QCD methods.

We also evolve the central strange quark mass value $m_s(\mu = 2 \text{ GeV}) = 100 \pm 25 \text{ MeV}$. We use as the energy scale the CM-reaction energy $\mu \simeq \sqrt{s}$ working in two loops. Some simplification is achieved by considering at temperature T the QCD scale $\mu \simeq 2\pi T$, thus $m_s(T) = m_s(\mu = 2\pi T)$ with $m_s(T = 318 \text{ MeV}) = 0.1 \text{ GeV}$. The actual temperature $T(t)$ and thus the time dependent values of the strange quark mass, are seen in the top panel of Fig. 8.

Fig. 8 illustrates in detail how a variation of the unknown initial chemical equilibration conditions impacts the final strangeness yield results. Since the entropy seen at the end of the reaction is already present at an early time, it is fixed as function of time and is the same for the different initial state scenarios explored. $T(\tau_0)$ is obtained (top panel) for a wide range of assumed initial gluon (and quark) occupancy $0.1 < \gamma_g(\tau_0) < 2.1$, in step of 0.5, shown in the middle panel by dashed lines.

Results for strangeness production at RHIC (left) and LHC (right) as function of proper time τ are shown in middle and bottom panels; the solid lines in middle panel show the resulting γ_s , and in the bottom panel s/S . Two results emerge: the value of γ_s at QGP hadronization is nearly independent of the initial conditions; the evolution of s/S in time is a universal curve. A large part of the difference between RHIC and LHC arises because the expansion lasts longer. At RHIC, the thermal strangeness production raises the value of s/S from 0.016 to 0.028, and at the LHC the thermal strangeness production raises s/S from 0.016 to 0.032. This 20% increase in relative strangeness yield has a highly significant impact on production of strange hadrons.

These results show that the observable s/S is dependent on the dynamics of dense matter evolution (and also QCD parameters α_s, m_s , but not on the internal structure of the QGP, and in particular not on the degree of chemical equilibration). At a fixed entropy yield, a plasma that has not yet reached chemical equilibrium is hotter. This higher T compensates

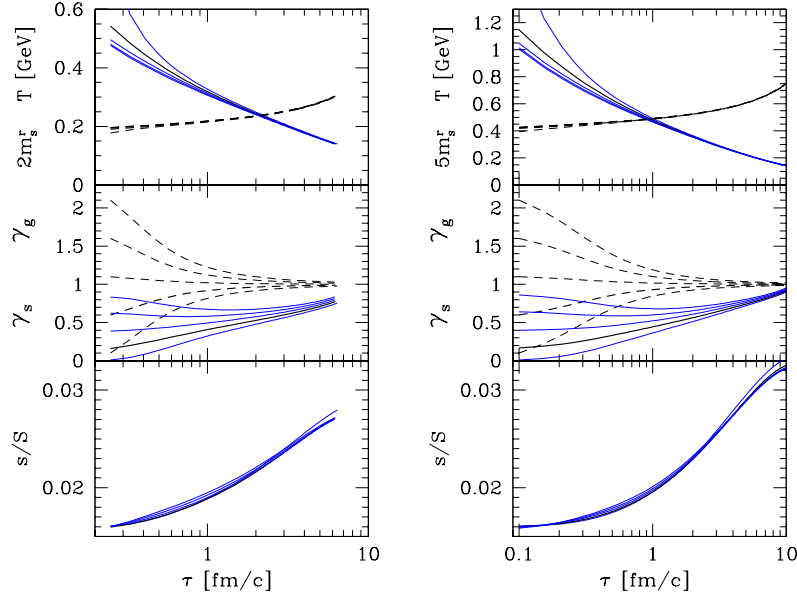


Fig. 8. Strangeness production at RHIC (left) and LHC (right) for the case of 5% most central collisions. s/S (bottom panel) and γ_s (solid lines middle panel) evolution as function of proper time τ . In this study, widely varying initial gluon conditions (γ_g dashed middle panel) constrained to same entropy content, and thus, varying temperature T (top panel), is presented. Volume expands according to $dV/dy = \pi[R_0 + \int v(\tau)d\tau]^2\tau$.

in strangeness production the lack of chemical equilibration, *i.e.*, $\gamma_G < 1$. Entropy is practically constant since the process of chemical equilibration does not produce significant amount of entropy [35], which is mostly produced in the process of thermal equilibration.

The final strangeness content expressed by s/S depends also on the initial entropy content, $dS(\tau_0)/dy$. This value can change both due to change in energy and centrality of the reaction. A scenario study shows that variation of centrality leaves us on the universal s/S curve seen in Fig. 8, but the freeze-out temperature is reached sooner for smaller volumes with smaller dS/dy , and thus, smaller s/S is achieved. A similar result is obtained when varying reaction energy. For this reason, we present in Fig. 9 the final s/S and γ_s as function of dS/dy . These two results, s/S and γ_s , will change independently under variation of strange quark mass, with γ_s remaining nearly unchanged and s/S changing. Considering different conditions for the volume evolution one can vary both s/S and γ_s by the same magnitude, 10–20%. We remind the reader that the γ_s discussed in this section is for the QGP phase while the γ_s discussed in hadronization analysis is for HG phase and is generally 2.5 times greater.

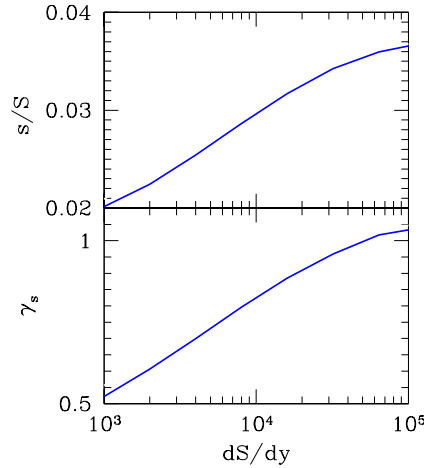


Fig. 9. s/S (top panel) and γ_s (bottom panel) as function of dS/dy .

7. Strange hadron resonances

Theoretical models of hadron production need to account in their study of particle spectra or/and hadron yields for the contribution originating in resonance decays. In the statistical hadronization, the production of hadron resonances is abundant. Within a particle “family”, particle yields with same valance quark content are in relation to each other well described by integrals of relativistic phase space, eventually corrected for rescattering [36]. The relative yields of, *e.g.*, $K^*(\bar{s}q)$ and $K(\bar{s}q)$, are controlled by the particle masses m_i , statistical weights (degeneracy) g_i and the hadronization temperature T . In the Boltzmann limit, one has (star denotes the resonance):

$$\frac{N^*}{N} = \frac{g^* m^{*2} K_2(m^*/T)}{g m^2 K_2(m/T)} \frac{|\overline{\mathcal{M}^*}|^2}{|\overline{\mathcal{M}}|^2}. \quad (12)$$

In the statistical hadronization model, the assumption made is that the matrix element $\mathcal{M}(E)$ is not strongly energy dependent (E is energy of particle produced). Thus, as shown above, the energy average factorizes. Moreover, one also expects that for most strongly interacting particles, the quantum strength saturates at its maximum, $|\mathcal{M}|^2 \rightarrow 1$, $|\mathcal{M}^*|^2 \rightarrow 1$, in the energy range in which most particles are produced (but not necessarily in some extreme corners of phase space where special situations prevail).

Resonance production is measured, in an experiment, directly by the decay product invariant mass method. Presence of these particle, and the fact that their 4-momenta add up to form invariant mass of the parent means that most if not all of the decay products do not significantly rescatter.

Except for special cases (ϕ , Ω , $\bar{\Omega}$) resonances contribute 50% and more of the yield of each hadron. When this is recognized in an analysis of experimental data, one finds that all particles are produced at the same temperature and that the yield temperature (chemical freeze-out) and spectral temperature (thermal freeze-out) are the same. This analysis was done for the maximal SPS energy [37], and the maximal RHIC energy [38]. Claims to the contrary rely on analysis which rescatter the resonance decay products such that all particles considered are forced to satisfy a thermal spectrum overlaid with flow from expansion dynamics. This, then, produces for different particles different freeze-out conditions of temperature and velocity. Such analysis is of course wrong as it presumes tacitly that not a single resonance should be observable by invariant mass method.

Putting aside the global analysis of data, we can argue qualitatively for single freeze-out, comparing the baryon and antibaryon m_{\perp} spectra as measured very precisely by WA97 and NA57 at SPS [39, 40], and STAR at RHIC [41, 42]. We note that if hadron gas were to surround at any relevant stage the plasma phase, such a symmetry could not arise in the presence of a baryon excess: the $\bar{\Lambda}$, $\bar{\Xi}$ annihilation is strongly momentum dependent, this should deplete the low momentum yield. This deforms the shape of the antihyperon spectra, as compared to the spectra of hyperons. More specifically, $\bar{\Xi}$ could annihilate on relatively abundant $N - \bar{N}$, $\Lambda - \bar{\Lambda}$, $\Sigma - \bar{\Sigma}$ (rather than the much less abundant $\Xi - \bar{\Xi}$), and yet the spectral m_{\perp} -distributions of $\bar{\Xi}$ are within a fraction of percent that is, measurement error, identical to Ξ . Absence of spectral deformation suggests that $\bar{\Xi}$ emerge directly and without significant rescattering.

Our working hypothesis is therefore, that hadronization of the QGP deconfined phase formed in high energy nuclear collisions at top SPS energy and RHIC energies is direct, fast (sudden) and occurs without significant sequel interactions. In this circumstance, the measurement of the relative yield of hadron resonances is a sensitive test of the statistical hadronization model (SHM) hypothesis and lays the foundation to the application of the SHM method in data analysis. One of the great successes of the chemical nonequilibrium particle yield analysis is the agreement with the experimental resonance yields. These, in particular, are at RHIC $K^*(892)$, $\Lambda(1520)$ [43, 44]. Our relatively low hadronization (chemical freeze-out) temperature makes this possible. More data is on the way and will keep us busy in coming years [45, 46].

We believe that the systematic study of resonance production can resolve the question about the reaction energy dependence of the freeze-out condition temperature. One could argue naively that this is simply the temperature at the quark-hadron transformation seen in lattice computations. This implies a smooth change with reaction energy, since temperature

rises smoothly while baryon density decreases. The maximum value of T is reached at highest reaction energy. However, since there is no sharp phase transition at small baryon density prevailing at LHC, RHIC and perhaps top SPS energy, this hypothesis contains an uncertainty: the value of cross-over temperature varies depending on observables considered. Moreover, among lattice results there is considerable difference in the range of interest for maximum T , with $T = 195 \pm 10$ MeV [47], and $T = 151 \pm 5$ MeV [48], at zero baryon density. In recent years, T has varied within these limits [49–51].

Our view is that freeze-out temperature is, to a large extent, influenced by the dynamics of the rapidly expanding fireball [52]:

- (a) When the collective flow occurs at parton level, the color charge flow, like a wind, pushes out the vacuum, adding to thermal pressure a dynamical component [53,54]. This can, in general, lead to supercooling and a sudden breakup of the fireball. We find that this can reduce the effective hadronization temperature by 20 MeV [53].
- (b) We also must consider the chemical composition of the hadronizing QGP. It is well known that the critical temperature is dependent on the flavor content. Thus, the degree of chemical equilibration of strange quark flavor influences the exact location of the boundary, and the nature of the transition. Because the degree of equilibration in the QGP depends on the collision energy, as does the collective expansion velocity, we cannot expect a simple hadronization scheme appropriate for the hadronization of nearly adiabatically expanding Universe. We can be nearly sure that the chemical conditions matter and can displace the transition temperature.

At highest heavy ion reaction energy, in chemical equilibrium models [55], one obtains chemical freeze-out temperature $T \sim 170$ MeV. Values as low as $T \sim 50$ MeV are reported at lowest reaction energies available. As the collision energy increases, the freeze-out temperature increases and the baryonic density (here baryonic chemical potential μ_B) decreases. Such an increase of freeze-out temperature with collision energy is expected on general grounds, since with increasing reaction energy a greater fraction of the energy is carried by mesons created in the collision, rather than pre-existing baryons [56].

There is no sign of any structure, in Fig. 10, when the reaction energy varies. The rather smooth hadronization curve makes it impossible to describe the experimental discontinuity in the ratio K^+/π^+ (see Fig. 6) and other related experimental features [27]. An effort was made to interpret this in terms of a shift from baryon to meson dominance [57] of the hadron yields. However, in the chemical equilibrium model, all observables including K^+/π^+ remain a smooth function of reaction energy, in contrast to the experimental results.

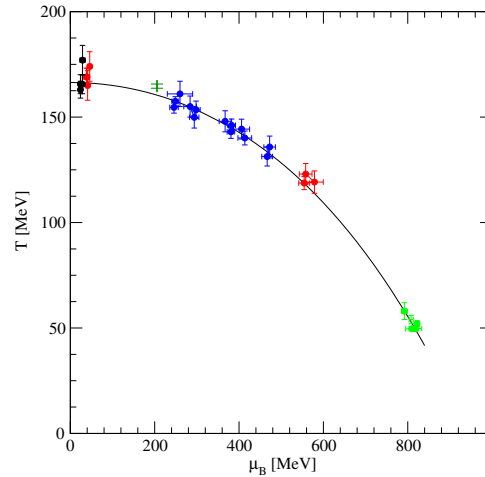


Fig. 10. Freeze-out boundary temperature T and baryo-chemical potential μ_B on reaction energy following from the chemical equilibrium hypothesis, after Ref. [55]. The line guides the eye.

The question of considerable importance is how we can find agreement on what the temperature of hadronization is, and be able to trace in the phase diagram the hadronization boundary, in a way that leads to general agreement. The disagreement is considerable. In Fig. 10, we see the situation proposed for the hadron system considered to be in absolute chemical equilibrium [55].

The systematic behavior of freeze-out condition in the T - μ_B plane allowing for $\gamma_q \neq 1$ is quite different [26], see Fig. 11. The two higher T values at right are for 20 A GeV (lowest CERN-SPS energy) and (furthest to right) 11.6 A GeV (highest BNL-AGS energy) reactions. In these two cases the source of particles is relatively large, dilute and strongly chemically under-saturated, and hotter than otherwise has been expected. Such a system could be a conventional hadron gas fireball that had not the time to chemically equilibrate. Other options were considered such as a phase of constituent massive quarks.

The higher temperature and lower density imply that at the time of freeze-out the fireball is not expanding as fast as found at higher reaction energies. Thus without doubt sudden hadronization does not apply here. The transition to the supercooled regime occurs and the phase space changes from chemically under-saturated ($\gamma_q < 1$) to chemically over-saturated ($\gamma_q > 1$) where the two dashed lines meet in Fig. 11. At heavy ion reaction energy below (*i.e.*, to right in Fig. 11) of this point, hadrons freeze-out with meson number enhanced with reference to antibaryon yield. Above 30 A GeV the antibaryon to meson yield is enhanced.

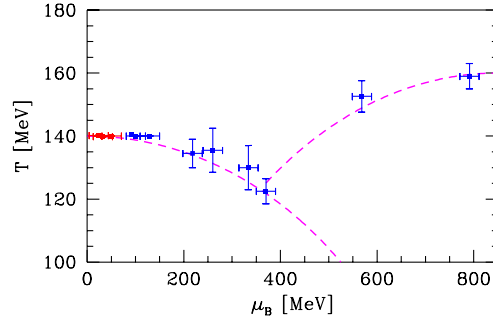


Fig. 11. Dependence of freeze-out temperature T and baryo-chemical potential μ_B on reaction energy in the non-equilibrium case [26]. The dashed lines guide the eye.

The relative resonance yield Eq. (12) is only dependent on the temperature of hadronization. Hence the relative yield of resonances will distinguish the two scenarios presented in Figs. 10 and 11 [58]. Torrieri *et al.* evaluated the relative yield of resonances along the two hadronization curves as function of reaction energy and have found that the behavior is practically opposite. Relative resonance yields in the equilibrium model rise monotonically with energy of heavy ion reaction. The nonequilibrium model implies overall a reduction of T with increasing heavy ion reaction energy, with a strong dip near to the “horn” energy. Moreover, and beyond the argument presented in [58], the visible resonance yield could be negligible at lowest SPS energies due to rescattering of decay products in absence of sudden hadronization.

8. Outlook

Rereading many experimental and theoretical works we have had an impression that there is more experimental data than theoretical effort in this very rich field. To our despair, much of the data analysis is scope-restricted and does not seek overall consistency. Authors of failed theoretical ideas do not come forward to withdraw. Their ideas live on, and are resurrected. Today, we see more confusion in the field than there has ever been. Unfortunately, this confusion is welcome in some quarters, simply because there is such good strangeness data, generating a very clear message, overshadowing other observables.

At SPS and RHIC, we see a chemically equilibrated strangeness rich s - q - g system. What we are not 100% sure of is, if this is the every-day quark-gluon plasma, though there is plenty of evidence that it is. We have discussed how the degree of chemical equilibration in QGP varies, with system size, and reaction energy. The result follows from glue-based strangeness production.

Entropy content seen in particle multiplicity, is for the most central and most energetic RHIC reactions just as QGP predicts — the ratio s/S measures directly the ratio of strange to all QGP degrees of freedom. At the 10% level, or better, it agrees with what one expects from the chemically equilibrated, interacting quark–gluon fluid.

Hadronization of the fireball of matter formed in heavy ion reactions leads to quite different spectra and yields of hadrons than we expect based on elementary pp reactions. This change in reaction mechanism favors, in particular, the production of multi strange baryons and antibaryons. The enhancement we see is what statistical recombination of quarks predicts, both as function of centrality and energy.

Many years ago, when the first ideas how to look for quark-matter were born, it seemed that the energy threshold to deconfinement could be low. Nucleons in nuclei seemed to be just barely retaining their individual identities. Just a little push and squeeze with a few GeV beam could perhaps be sufficient to lead to deconfinement [4]. This is where we are today, after a long and dramatic excursion to the very high RHIC energies: Strange antibaryon enhancement suggests that at least down to 40 A GeV we have s - q - g -matter. The simplest of all possible observables, the K^+/π^+ ratio shows a threshold between 20 and 30 A GeV projectile energy.

Let us cross our fingers that RHIC can and will run at a few GeV per beam. The existent detectors would in this environment produce very precise data on strange hadron production, including resonances, and have nearly full coverage in phase space. This would with certainty resolve any doubt about QGP, both its formation and threshold as function of centrality and reaction energy. This will further lead to detailed understanding of the phases of QCD. This work will complement the LHC based study of perturbative QGP.

Supported by a grant from the United States Department of Energy, DE-FG03-95ER40937. Laboratoire de Physique Théorique et Hautes Energies, LPTHE, at University Paris 6 and 7 is supported by CNRS as Unité Mixte de Recherche, UMR7589.

REFERENCES

- [1] J. Kapusta, B. Müller, J. Rafelski, *Quark–Gluon Plasma: Theoretical Foundations* (An annotated reprint collection) Elsevier, Amsterdam 2003.
- [2] G. Torrieri, S. Steinke, W. Broniowski, W. Florkowski, J. Letessier, J. Rafelski, *Comput. Phys. Commun.* **167**, 229 (2005); G. Torrieri, S. Jeon, J. Letessier, J. Rafelski, *Comput. Phys. Commun.* **175**, 635 (2006).

- [3] J. Rafelski, R. Hagedorn, CERN-TH-2969, in H. Satz, ed. *Statistical Mechanics of Quarks and Hadrons*, North-Holland, ISBN 0444862277, Amsterdam 1981, pp. 253–272.
- [4] J. Rafelski, Proceedings of *Future Relativistic Heavy Ion Experiments* 1980, eds. R. Bock, R. Stock, published by GSI, Darmstadt 1981, GSI Report 1981–86, pp. 282–324; scan available at:
<http://www.physics.arizona.edu/~rafelski/PS/81GSIPaperJR.pdf>
- [5] J. Rafelski, J. Letessier, A. Tounsi, *Acta Phys. Pol. B* **27**, 1037 (1996) [nucl-th/0209080 (late submission to make paper accessible)].
- [6] C. Greiner, P. Koch, H. Stoecker, *Phys. Rev. Lett.* **58**, 1825 (1987).
- [7] C. Alt *et al.* [NA49 Collaboration], *Phys. Rev.* **C73**, 044910 (2006) and private communication by M. Mitrovski.
- [8] F. Antinori *et al.* [NA57 Collaboration], *J. Phys. G* **32**, 427 (2006).
- [9] P. Koch, B. Muller, J. Rafelski, *Phys. Rep.* **142**, 167 (1986).
- [10] F. Antinori *et al.* [NA57 Collaboration], *Phys. Lett.* **B595**, 68 (2004).
- [11] F. Antinori *et al.*, *AIP Conf. Proc.* **828**, 333 (2006).
- [12] J. Rafelski, J. Letessier, *Acta Phys. Pol. B* **34**, 5791 (2003).
- [13] J. Rafelski, J. Letessier, *Acta Phys. Pol. B* **30**, 3559 (1999).
- [14] H. Caines, nucl-ex/0609004.
- [15] M.K. Mitrovski *et al.* [NA49 Collaboration], nucl-ex/0606004, *J. Phys. G* in press.
- [16] J. Letessier, J. Rafelski, *Phys. Rev.* **C73**, 014902 (2006).
- [17] H. Caines [STAR Collaboration], *J. Phys. G* **31**, S1057 (2005).
- [18] S.S. Adler *et al.* [PHENIX Collaboration], *Phys. Rev.* **C69**, 034909 (2004).
- [19] J. Rafelski, J. Letessier, G. Torrieri, *Phys. Rev.* **C72**, 024905 (2005).
- [20] K. Redlich, A. Tounsi, *Eur. Phys. J.* **C24**, 589 (2002).
- [21] C. Adler *et al.* [STAR Collaboration], *Phys. Rev. Lett.* **89**, 092301 (2002).
- [22] J. Adams *et al.* [STAR Collaboration], *Phys. Rev. Lett.* **92**, 112301 (2004).
- [23] J. Adams *et al.* [STAR Collaboration], *Phys. Lett.* **B595**, 143 (2004).
- [24] R.J. Fries, B. Muller, C. Nonaka, S.A. Bass, *Phys. Rev. Lett.* **90**, 202303 (2003); *Phys. Rev.* **C68**, 044902 (2003).
- [25] R.C. Hwa, C.B. Yang, *Phys. Rev.* **C67**, 034902 (2003).
- [26] J. Letessier, J. Rafelski, nucl-th/0504028, submitted to *Phys. Rev. C*.
- [27] M. Gazdzicki *et al.* [NA49 Collaboration], *J. Phys. G* **30**, S701 (2004) and commented compilation of NA49 results, private communication.
- [28] M. van Leeuwen, Compilation of NA49 results as function of collision energy, private communication (2003).
- [29] N.K. Glendenning, J. Rafelski, *Phys. Rev.* **C31**, 823 (1985).
- [30] H.B. Zhang [STAR Collaboration], nucl-ex/0403010; J. Adams [STAR Collaboration], *Phys. Rev.* **C71**, 064902 (2005).

- [31] J. Adams *et al.* [STAR Collaboration], *Phys. Lett.* **B612**, 181 (2005).
- [32] J. Letessier, J. Rafelski, G. Torrieri, [nucl-th/0411047](#).
- [33] J. Letessier, J. Rafelski, [nucl-th/0602047](#).
- [34] S.A. Chin, A.K. Kerman, *Phys. Rev. Lett.* **43**, 1292 (1979).
- [35] J. Letessier, J. Rafelski, A. Tounsi, *Phys. Rev.* **C50**, 406 (1994).
- [36] J. Rafelski, J. Letessier, G. Torrieri, *Phys. Rev.* **C64**, 054907 (2001); Erratum: **C65**, 069902 (2002).
- [37] G. Torrieri, J. Rafelski, *New J. Phys.* **3**, 12 (2001).
- [38] W. Florkowski, *Nucl. Phys.* **A774**, 179 (2006); W. Broniowski, W. Florkowski, *Phys. Rev. Lett.* **87**, 272302 (2001); *Phys. Rev.* **C65**, 064905 (2002).
- [39] F. Antinori *et al.* [WA97 Collaboration], *Eur. Phys. J.* **C14**, 633 (2000).
- [40] G.E. Bruno [NA57 Collaboration], *J. Phys. G* **31**, S127 (2005).
- [41] J. Adams *et al.* [STAR Collaboration], *Phys. Rev. Lett.* **92**, 182301 (2004).
- [42] J. Adams *et al.* [STAR Collaboration], [nucl-ex/0606014](#).
- [43] C. Markert, G. Torrieri, J. Rafelski, [hep-ph/0206260](#), in *AIP Conference Proceedings* **631**, pp. 533–552.
- [44] C. Markert, *J. Phys. G* **31**, S169 (2005).
- [45] J. Adams *et al.* [STAR Collaboration], *Phys. Rev. Lett.* **97**, 132301 (2006).
- [46] S. Salur, [nucl-ex/0606002](#), *J. Phys. G* in press.
- [47] M. Cheng *et al.*, [hep-lat/0608013](#).
- [48] Y. Aoki, Z. Fodor, S.D. Katz, K.K. Szabo, [hep-lat/0609068](#).
- [49] F. Karsch, *Nucl. Phys.* **A698**, 199 (2002).
- [50] Z. Fodor, S.D. Katz, *J. High. Energy Phys.* **0404**, 050 (2004).
- [51] F. Karsch, E. Laermann, [hep-lat/0305025](#); R.C. Hwa *et al.*, *Quark Gluon Plasma III*, pp. 1–59, World Scientific, Singapore 2004.
- [52] J. Rafelski, J. Letessier *Eur. Phys. J.* **A29**, 107 (2006).
- [53] J. Rafelski, J. Letessier, *Phys. Rev. Lett.* **85**, 4695 (2000).
- [54] T. Csorgo, J. Zimanyi, *Heavy Ion Phys.* **17**, 281 (2003).
- [55] J. Cleymans, H. Oeschler, K. Redlich, S. Wheaton, [hep-ph/0607164](#).
- [56] R. Hagedorn, J. Rafelski, *Phys. Lett.* **B97**, 136 (1980).
- [57] J. Cleymans, H. Oeschler, K. Redlich, S. Wheaton, [hep-ph/0504065](#).
- [58] G. Torrieri, J. Rafelski, [nucl-th/0608061](#).